Investigations on the Bragg grating recording in all-silica, standard and microstructured optical fibers using 248 nm, 5 ps laser radiation

S. Pissadakis Institute of Electronic Structure and Laser, Foundation for Research and Technology – Hellas, Greece
pissas@iesl.forth.gr

M. Livitziis Institute of Electronic Structure and Laser, Foundation for Research and Technology – Hellas, Greece

G. D. Tsibidis Institute of Electronic Structure and Laser, Foundation for Research and Technology – Hellas, Greece

The fabrication of Bragg reflectors in hydrogenated, all-silica, fluorine cladding depressed and microstructured optical fibers using 248 nm, 5 ps laser radiation, is investigated here. Comparative Bragg grating recordings are performed in both optical fibers, for investigating effects related to the scattering induced by the capillary micro-structure, to the photosensitivity and index engineering yield. Further, finite difference time domain method is employed for simulating the scattering from the above capillary structure and the nominal intensity reaching the fiber core for side-illumination. The maximum modulated refractive index changes inscribed in the standard, step-index fiber were of the order of 8.3×10^{-5}, while the maximum refractive index changes inscribed in one of the microstructured optical fibers was 32% lower and 5.7×10^{-5}, for nominal pulse intensities of 20 GW/cm^2 and modest accumulated energy densities. [DOI: 10.2971/jeos.2009.09049]

Keywords: fiber Bragg gratings, microstructured optical fibres, silica, photosensitivity, hydrogenation

1 INTRODUCTION

The straightforward and high yield inscription of strong, photosensitive Bragg reflectors and long-period periodicities in all-silica microstructured optical fibers (MOFs) [1], is a significant step towards the development of functional photonic devices based on these unique optical platforms. Focusing on the case of Bragg reflectors, there are two fundamental parameters that dominate the yield of the inscription process: the low photosensitivity of the pristine silicate glass matrix, and the scattering effects induced by the guiding capillary microstructure.

Dealing with the first parameter, that of the material photosensitivity, the successful inscription of large refractive index changes into pure silicate glasses remains a significant material science issue. Fused silica is an optical material of 9.3 eV bandgap, and low intrinsic defect concentration, while exhibiting a high resistance to radiation induced damage. These unique material characteristics prompt the use of high intensity and photon energy lasers as a promising route for the inscription of exploitable refractive index changes in that glass matrix. There have been several approaches in the photosensitivity and refractive index engineering of pure silicate glass, which are summarized either in the use of 193 nm nanosecond excimer radiation [2], or in the use of 800 nm [3], 248 nm [4] and 267 nm [5] femtosecond laser radiation. For increasing the ultraviolet photosensitivity of the exposed silicate matrix, hydrogen loading at high pressures is a common technique that is broadly adopted. Bragg and long-period gratings have been recorded by using the above approaches inside fluorine depressed cladding [2] and microstructured [6]–[8] all-silica optical fibers.

Furthermore, the scattering loss induced by the capillary microstructure to the recording laser beam, renders the inscription of short period Bragg reflectors a difficult engineering problem of pulsed light propagation through a semi-periodically stratified medium. Simple ray tracing, finite element and finite difference time domain [10]–[12] and multipole formulation [13] methods have been employed for describing the laser beam intensity propagation and spatial distribution during side-illumination, providing results of different accuracy and physical insight. Also recently, there have been experimental studies on the impact of grating growth trend upon the rotation positioning of a highly-asymmetric, birefringent fibre, with respect to the incoming beam [14]. However, few data have been given for the intensity topology inside the MOF core and its impact on the photosensitivity behaviour of the exposed fiber. Also, there have not been any comparative exposures between step-index and microstuctured all-silica fibers of similar composition.

Here in, we present the use of 248 nm, 5 ps laser radiation for the performing comparative exposures of Bragg reflectors in two all-silica, hydrogen loaded commercial fibers: one step-index fluorine depressed cladding and a microstructured optical fiber. Our study constitutes a first step towards the investigation of the scattering role of the guiding capillaries in the overall grating recording yield in hydrogenated, all-silica optical fibers. For investigating the above, we employ a finite difference time domain method (FDTD) for gaining some insight into the spatial distribution of the side illuminating laser beam inside the core-cladding complex, for the cases of the

Received October 11, 2009; published December 10, 2009 ISSN 1990-2573

Z-fiber and the ESM-12-01 fiber. Our approach refers to idealized cases, where the fiber exhibits known orientation with respect to the laser beam. This analysis will be used for obtaining some characteristic figures related to the amount of light that reaches the core of the fibers examined here; which in turn can be used as a rough guide for justifying/understanding the experimental results.

Focusing on the photosensitivity side, the use of 248 nm, 5 ps laser radiation provides specific advantages compared to the previous art. The energy sum of two 248 nm photons is above the bandgap of the silicate glass, leading to significant two-photon absorption coefficients, compared to longer wavelengths, i.e. 267 nm [4, 15]. That higher two-photon absorption coefficient in combination with the occurrence of intensities of the order of tens of GW/cm^2, can lead to the efficient grating recording in the hydrogenated silica, utilising modest radiation doses and longer laser pulses. Moreover, the 248 nm photon highly overlaps with the oxygen deficiency and hydrogen based defect centers absorbing at 5 eV vicinity, increasing the possibility of single photon related excitations, which in turn may also contribute to the overall photosensitivity yield [16, 17].

2 EXPERIMENTAL

For Bragg grating inscription, a hybrid, Lambda-Physik distributed feedback dye laser/excimer laser emitting at 248 nm 5 ps pulses, was used. The flux contrast ratio between the emitted picosecond pulse and the nanosecond tail is greater than 95%. The laser delivered a 3 cm $\times$ 3 cm beam, of 20 mJ energy per pulse, at a repetition rate of $\approx$ 10 Hz. The polarisation of the laser beam emitted is vertical, at a rate of 93%. The beam delivery setup has been described before elsewhere [4]. A 1073.5 nm period fused silica phase mask, optimized for the 248 nm wavelength, was used. The grating transmission was monitored in real time using a broadband superluminescent diode source and an optical spectrum analyzer. The all-silica fibers exposed, were the fluorine depressed cladding Z-fiber, fabricated by Sumitomo and the micro-structured, endlessly single-mode ESM-12-01, optical fiber fabricated by former Blazephotonics. Both of the above fibers are considered to be of "dry" composition exhibiting OH concentration less than 1 ppm. The manufacturer did not disclose any information related to the fluorine doping concentration and the core diameter of the Z-fiber, except that of the cut-off wavelength (1460 nm) [18]. A measurement of the core diameter was performed using white light optical microscopy, providing a rough estimation of $\approx$ 9 μm. Other reports claim that the NA of Z-fiber is of the order of 0.12 [19], resulting in a core diameter of 9.3 μm and a mode confinement value Γ [20] of 0.79, a value quite close to that of SMF-28. The ESM-12-01 fiber has a total of 54 air holes with a diameter of 3.68 μm each and 8 μm center to center distance between them. The fiber has a solid core of 12 μm diameter and attenuation at 1550 nm of less than 0.8 dB/km [21]. The mode confinement factor for the ESM-12-01 fiber was calculated using the FDTD method at 0.977, approximately. All fibers were hydrogenated at 130 atm for 15 days at 25°C prior to the exposure, while for the case of the micro-structured fiber both ends were spliced to standard telecom fiber, in order to allow a slower hydrogen out-diffusion during grating recording [10].

For the case of the microstructured fiber the out-diffusion time of hydrogen from the central core is considered to be short and highly dependent on the condition of the side splices to the SMF-28 fiber. A rough calculation of the hydrogen out-diffusion time at room temperature, for reaching concentrations of the order of 5% of the saturated solubility, for a 5 μm radius fiber core leads to a figure of 120 min, approximately [10, 22]. Most of the grating exposures were carried out after a "dead" time interval of $\approx$ 15 min after unloading the fiber from the hydrogen chamber. The above time constrains frustrated the precise axial alignment of the fiber capillary microstructure with respect to the incoming laser beam. A low-power, alignment was performed along the vertical axis of the fiber, by finding the point where the magnitude of the scattered ultraviolet light from the capillary array after the fiber, was minimum [3].

3 SIDE-ILLUMINATION SIMULATIONS OF THE STANDARD AND MICROSTRUCTURED OPTICAL FIBERS USING FDTD

Average energy densities of the order of $\approx$ 100 mJ/cm^2 ($\approx$ 20 GW/cm^2), as these measured after the phase mask, were used for the experiments performed. The energy density of the ultraviolet beam reaching the fiber core, is expected to be significantly lower than that measured before the fiber curved interface using a joulemeter. This is attributed to two experimental parameters: (a) the scattering and interference effects that take place in the capillary superstructure, and (b) the linear and non-linear absorption that occurs in the capillary and cladding section, which in turn is directly associated with the spatial distribution of the beam intensity in the fiber area. We have analyzed in the past the beam intensity distribution into the fiber core considering the optical design of our experimental setup (pulse duration and bandwidth, wavelength, cylindrical lens focal length and relative fiber position, phase mask thickness and diffraction angle) and several angular orientations of the MOF, by using simple ray tracing software [23].

We utilize a commercial FDTD software package for conducting the pulse propagation simulations in the specified fiber geometries [24]. In particular, a fiber of cladding diameter 125 μm was illuminated by a Gaussian modulated continuous TE-polarised beam directed perpendicularly to the fiber. Due to memory constraints the simulation was carried utilizing a 2-D approach, therefore, for normal incidence of the laser beam with respect to the longitudinal fiber axis. A square observation area of 126 μm $\times$ 126 μm was chosen to cover the whole fiber layout. The refractive index of the hydrogenated silica matrix and the linear absorption coefficient for the "dry" hydrogenated silica for the 248 nm wavelength, utilised in the simulations carried out herein, were 1.507450 and 60×10^{-4} cm^{-1} [25], respectively. The intensity snapshots presented have been evaluated for a specific time interval that is twice long than the time the light needs to cover the fibre

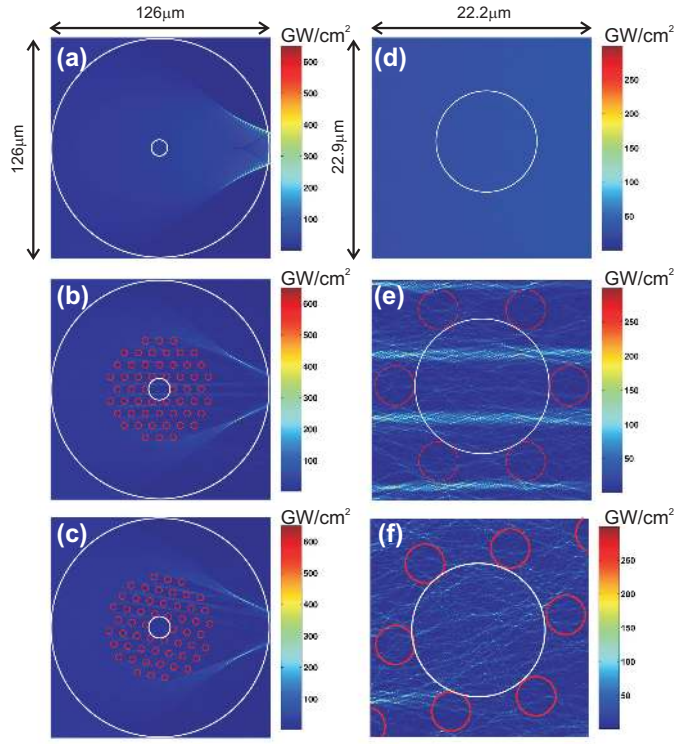

FIG. 1 Simulation results of the spatial distribution of the Pointing vector S using the FDTD method for the case of the Z-fiber; and that of the ESM-12-01 for 0° and 10° rotation angles. The outer and inner white circles define the fiber cladding and core, respectively. The red circles define the spatial boundaries of the individual capillaries. The color-bar, corresponds to the scale of the values of the Poynting vector S measured in GW/cm². (a), (d) Simulation of the side illumination for the equivalent structure corresponding to the Z-fiber; (b) (e) the case of ESM-12-01 fiber for 0°; and (c), (f) 10° angular rotation with respect to ΓK axis. The (a), (b), (c) images correspond to views of the whole fiber area with dimensions 126 μm × 126 μm. The (d), (e), (f) images correspond to magnified views of a rectangular region 22.2 μm × 22.9 μm in the vicinity of the fiber core of the above optical fibers, for core diameters 9 μm and 12 μm, respectively.

length and the first back-reflection from the further fiber-end reaches the initial source, namely ≈ 0.9 ps. In such an approach, the contribution of the back-reflection components (by means of phase and intensity) emerging from the refractive index discontinuities are encountered in the actual intensity snapshot. The software package we used had not the capability of handling non-linear absorption effects triggered during 5 ps irradiations. Therefore, the simulation results presented herein do not include such intensity dependent correction.

The side-illumination simulation was conducted for various orientations of the MOF with respect to rotational symmetry around the longitudinal fiber axis. Further, a fiber rod which has the same refractive index and linear absorption such as the hydrogenated silica was simulated under the same irradiation conditions. The last was performed for obtaining similar type of results for the intensity distribution profile in the core vicinity of the standard fluorine depressed fiber; as well as, for illustrating the role of the curved fiber geometry and the capillary scattering effects. The field amplitude used for excitation in both cases was corresponding to a laser beam intensity of 20 GW/cm^2. The 2D plot of the magnitude of the Pointing vector S, obtained using the FDTD method for the two fibers simulated are presented in Figure 1(a)–1(f). Figure 1(a) shows the side illumination focusing effects that take place in a standard all-silica optical fiber cylinder, in the absence of the guiding capillaries. Accordingly, Figure 1(b) and 1(c) illustrate the scattering effects due to the capillary superstructure, for the case of the ESM-12-01 fiber at 0° and 10° orientations, with respect to the ΓK axis [13].

From a first view, the side-illumination simulations exhibit predominant similarities: a spherical aberration caustic is generated by the cylindrical interface of the fiber cladding, which in turn is short-focused at the back-side of the fiber complex. Further, at specific points of the spherical aberration caustic the local field intensities are of the order of several hundred GW/cm^2, for all the fiber geometries simulated. For the case of the microstructured fiber, the most significant differences arise from the existence of the capillary array, which directly affects the laser energy density distribution inside its central core. An enlarged view (22.2 μm × 22.9 μm) of the spatial distribution of the Poynting vector S in the neighbourhood of the fiber core for several angular orientations for the two fibers are illustrated in Figure 1(d)–1(f). In comparison to the pattern inside the core of the Z-fiber (Figure 1(d)) scattering effects occur for the ESM-12-01, (Figure 1(e)) fiber that result from the capillary microstructure. While the average intensity observed in the central area of the cylindrical fiber is 30.4 GW/cm^2 (see Table 1), the corresponding one for the ESM-12-01 at 0° is 18.7 GW/cm^2; a figure 2.5 times lower. The

Rotation	Fiber type	Intensities calculated for the core area (GW/cm)^2		
		I_{Mean}	I_{Max}	I_{Min}
0°	Z-Fiber	30.4	32.1	29.3
	ESM-12-01	18.7	70.1	10.6
10°	ESM-12-01	14.5	28.1	2.5

TABLE 1 Intensities calculated for the core area (GW/cm²), for different rotation angles and for the Z and ESM-12-01 fibres.

simulation for that angle yields a decrease by 38% to the average power that reaches the core of the ESM-12-01 fiber compared to the Z-fiber, which emphasises the importance of the scattering effects due to the air capillaries. Accordingly, the side-illumination results presented for the angular rotation of 10° show a smooth intensity distribution inside ESM-12-01 fiber core, without prominent "hot-spot" points. Figure 2 summarizes simulated data over one 60° rotation with respect to the ΓK axis. Simulated results in the range 0°-60° are reflected at the 30° point due to the symmetry the fiber around the 30° axis. Furthermore, a rotation of the ESM-12-01 fiber by 30° with respect to the ΓK axis leads to a 41% decrease of the average power inside the fiber (see Figure 2), compared with the corresponding intensity for 0°. This angle corresponds to the minimum average value of power that reaches the core of the ESM-12-01 fiber. The intensity of the laser beam propagating in the core of the ESM-12-01 fiber exhibits a complex shape spatial distribution of pronounced singularities and low-intensity areas. To estimate the magnitude of the singularities, the Poynting vector maximum values are sampled in a box of 0.2 μm around the position of the maximum or minimum related point (see Table 1). It is worthy mentioning

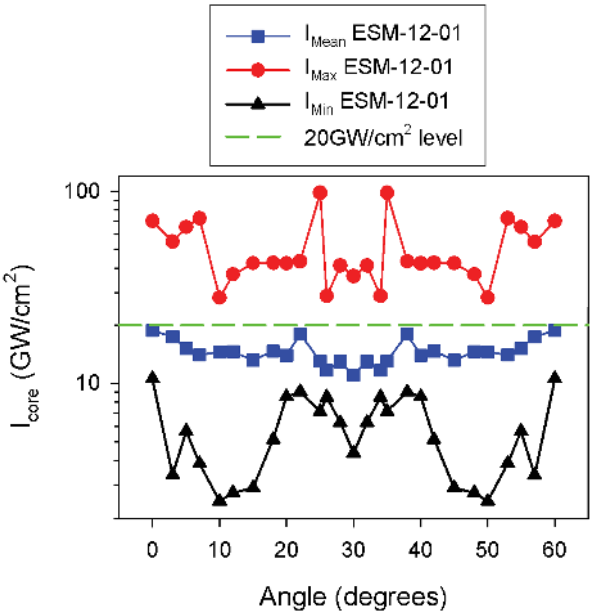

FIG. 2 Intensity figure in the core area I_{core} versus rotational angle with respect to the ΓK axis for the ESM-12-01 microstructured optical fiber. I_{Mean}: Averaged intensity. I_{Max}: Maximum intensity. I_{Min}: minimum intensity. The I_{Mean} values have been evaluated for the circular areas presented in Fig.1. The I_{Max} and I_{Min} figures have been sampled for a square patch of 0.2 μm side, around the maximum and minimum points, respectively. The green dash line refers to input pulse intensity as that measured before reaching the fiber complex.

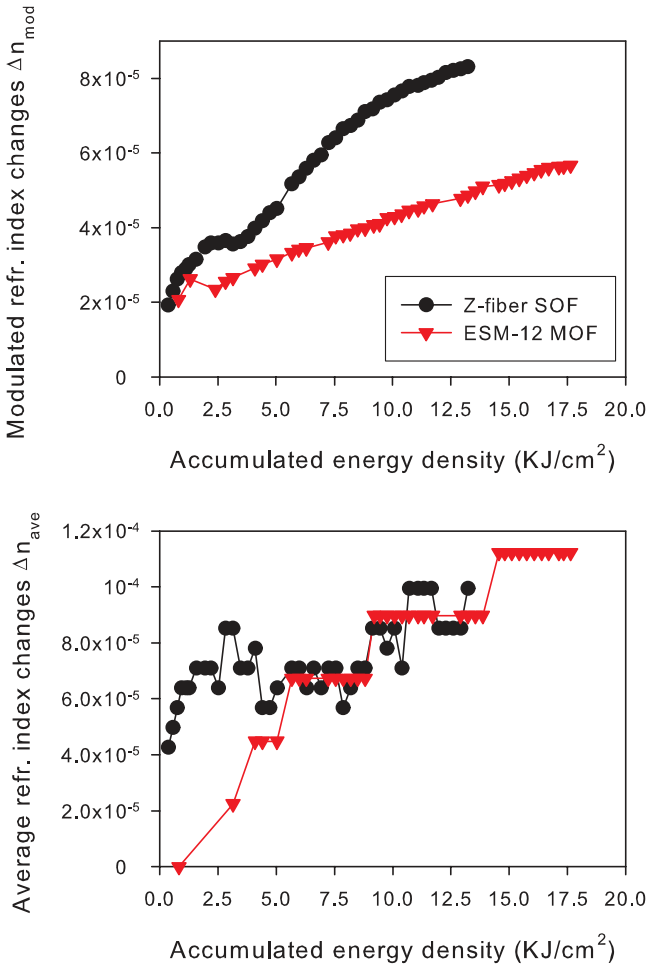

FIG. 3 Modulated Δn_{mod} and Average Δn_{ave} refractive index changes versus accumulated energy density doses for grating recordings in the standard step-index optical fiber (SOF) Z-fiber, and in the microstructured optical fiber (MOF) EMS-12-01. The refractive index data have been normalized to the corresponding mode confinement factor calculated for each fiber exposed.

the similarity on the general trend and I_{Mean} coordinates, between the data of Figure 2 and those presented by Marshall *et al.* where a different numerical/physical approach is followed and a smaller width scanning beam is adopted [13].

As shown in the Figure 2 and Table 1, the local field intensity in the core of the MOF reach maximum values of the order of 97.9 GW/cm^2 which are 205% higher than the maximum value in the absence of the capillaries. In photosensitivity and index engineering terms, both the I_{Max} and I_{Min} quantities are significant: at extreme intensity points the photosensitivity yield is boosted and sometimes the material may be locally damaged, while at low-intensity areas the transparent core material may remain almost intact. On the other hand, the I_{Mean} figure provides an average value for estimating intensity yield dissipated into the fiber core for assisting comparison. The significance of I_{Max} and I_{Min} intensity figures becomes even greater in the case of two-photon absorption mechanisms, where the refractive index changes induced are dependent upon the second power of the local intensity [4].

4 RESULTS ON THE BRAGG GRATING RECORDING IN THE STANDARD AND MICROSTRUCTURED OPTICAL FIBER

The modulated Δn_{mod} and average Δn_{ave} refractive index changes measured in the gratings inscribed in the Z-fiber and the ESM-12-01 MOF versus accumulated energy density, for pulse energy of 100 mJ/cm^2 (measured before the fiber complex), are presented in Figure 3. The above nominal intensity figure is used in order to allow easy comparison with other studies presented [2, 4]–[7]. The highest modulated refractive index changes are obtained for the case of the fluorine-depressed cladding Z-fiber, and are of the order of 8.3×10^{-5}. Accordingly, the average refractive index changes measured for the Z-fiber were $\approx 1.0 \times 10^{-4}$. Furthermore, the grating growth evolution in the same fiber appears to be non-monotonic, exhibiting an observable slope change for 3.15 kJ/cm^2 accumulated energy density. That anomaly may indicate the occurrence of a manifold underlying photosensitivity mechanism, which possibly may include some contribution from stresses and singularities that preferentially take place at the fluorinated silica core-cladding interface [26]. Also, the fluorine cladding is expected to be of lower photosensitivity than the pristine core [27], therefore, we estimate that the majority of the UV induced refractive index changes are confined in the core area. On the other hand, the grating recording trend of the all-silica MOF exhibit similar linear-like growth characteristics. The grating recorded in the ESM-12-01 fiber saturates for greater accumulated energy densities, while the refractive index changes obtained are of the order of 5.7×10^{-5}. Another interesting finding is related to the trend of the average refractive index changes Δn_{ave} inscribed in the current fibers. These data are characterized by an irregularly

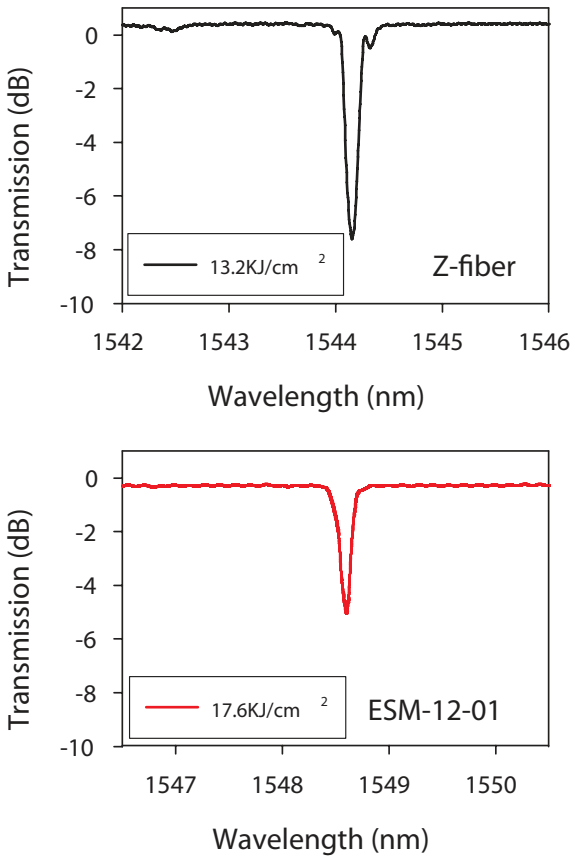

FIG. 4 Transmission spectra of Bragg gratings inscribed in the standard optical fiber (SOF) Z-fiber, and in the microstructured optical fiber (MOF) EMS-12-01, using 248 nm, 5 ps laser radiation. Grating length for all cases: 1 cm.

varying behaviour versus the energy dose; wherein the Bragg wavelength of the inscribed gratings either remained "frozen" during exposure or it is subjected to abrupt spectral shifts (see the data for the ESM-12-01 fiber). Such behaviour is usually observed during Type IIA grating recording, where strain and compaction effects induce opposite sign refractive index changes. Transmission spectra of the gratings inscribed in the aforementioned fibers are presented in Figure 4. The grating notches presented are scattered from 1 cm long gratings, without exhibiting any significant spectral distortions associated with stitching errors. In general, the exposure to the ultraviolet radiation resulted in no change of the out-resonance transmission level, denoting the occurrence of a low-damage recording process, especially for the case of the fluorine doped fiber, where damage can be located at the core cladding interface. Also, for the case of the MOF, no other broadband spectral notches located at shorter wavelengths were observed [9], corresponding to coupling to radiation modes, and induced by shallow, relief structures generated inside the fiber capillaries by accumulated compaction effects.

The experimental and simulation results presented above may give rise to specific questions related to the hydrogenated silica photosensitivity using 248 nm wavelength and picosecond pulses. While the maximum intensities dissipated in the fibre cores are at a sub-100 GW/cm^2 level, contrary to those generated by shorter pulse durations [5, 7], the refractive index yields obtained can be significant, for the energy density doses applied.

Generally, the primary underlying photosensitivity mechanism for the case of the silicate glass under deep ultraviolet laser irradiation is believed to be that of volume modification, generated by extensive bond cleaving and re-arrangements in the glass network. However, cross-sectional stress measurements performed in hydrogenated silicate fibres exposed using 264 nm, 220 fs laser radiation revealed that the main refractive index contribution for such material and exposure condition emerges from colour centre formation rather than compaction [28]. Moreover, Smith *et al.* [17] presented that volume expansion may take place in hydrogenated silica glass in addition to photorefractive effects, under specific energy density and dose condition exposures, using 248 nm, nanosecond excimer laser radiation. We assert that both colour centre formation and volume modification processes may take place in the 248 nm, 5 ps grating exposures. The underlying physical mechanism for both processes is associated with the high two-photon absorption coefficient of silicate glass at the 248 nm wavelength, which is $\approx 4.5 \times 10^{-11}$ cm/W [15], a figure 2.5 times greater than that of the longer 264 nm wavelength. For a typical local intensity of 40 GW/cm^2 at the bright fringe of interference, the nominal absorption related with two-photon effects is estimated to be 1.8 cm^{-1}; more than 100 times greater than that of the single photon absorption of the pristine silicate glass at that wavelength (namely, 0.016 cm^{-1}) [29]. Thus, two-photon absorption effects are expected to dominate the inscription process. An additional question is related to the sign of the refractive index changes induced. After examining the oscillating Δn_{ave} data, we believe that negative sign refractive index changes may occur in the grating exposures presented here, however, we cannot comment further on their actual strength and dependence upon energy dose. Focusing on the microstructured fibers exposures and further accounting the claims of reference [17], we speculate that the refractive index changes inscribed in the fiber core and cladding may be of alternating sign, depending upon the local intensity and accumulated dose figure. In such a case, the profile of the laser induced refractive index changes can be of complex topology, while local strains may also be generated due to abrupt variations in the refractive index.

5 CONCLUSIONS

We have presented the inscription of Bragg gratings in hydrogenated, step-index and microstructured all-silica optical fibers, using 248 nm, 5 ps laser radiation, by applying nominal intensities of the order of 20 GW/cm^2. For investigating the scattering effects induced in the side-illuminating laser beam by the capillaries; and the corresponding intensities reaching the guiding cores, for all the fiber geometries considered, we utilized a finite difference time domain method. The capillary micro-structures appear to induce significant scattering losses limiting the amount of average intensity that reaches the fibre core, compared to the values for a standard step-index all silica fiber. Therefore, the average intensities applied for efficient grating recording can be substantially lower than those measured before the fibre end-face and being of the order of few GW/cm^2. Moreover, a two-photon absorption mechanism is asserted to primarily drive the inscription process using the specific wavelength and pulse duration. Greater de-

tail theoretical results on the effect of side-illumination conditions on the grating growth characteristics for single- and multi-photon absorption processes, and for the fundamental and higher order modes, will be presented elsewhere.

ACKNOWLEDGEMENTS

Experiments were carried out at the Ultraviolet Laser Facility operating at FORTH-IESL with support from the EU through the Research Infrastructures activity of FP6 (Project: Laserlab-Europe; Contract No: RII3-CT-2003-506350). The authors would like to thank Dr Richard Zhang (Optiwave Systems Inc.) for his critical advise with FDTD simulations, as well as, Georgios Violakis for performing initial trials with that software tool. S. Pissadakis specially acknowledges Savas Georgiou (FORTH-IESL) for stimulating discussions and Andrew Bayram (Sumitomo Electric Europe Ltd.) for kindly supplying the F-doped Z-fiber.

References

[1] T. A. Birks, J. C. Knight, and P. S. J. Russell, "Endlessly single-mode photonic crystal fiber" Opt. Lett. **22**, 961–963 (1997).

[2] J. Albert, M. Fokine, and W. Margulis, "Grating formation in pure silica-core fibers" Opt. Lett. **27**, 809–811 (2002).

[3] S. J. Mihailov, D. Grobnic, H. Ding, C. W. Smelser, and J. Broeng, "Femtosecond IR laser fabrication of Bragg gratings in photonic crystal fibers and tapers" IEEE Photonic. Tech. L. **18**, 1837–1839 (2006).

[4] M. Livitziis, and S. Pissadakis, "Bragg grating recording in low-defect optical fibers using ultraviolet femtosecond radiation and a double-phase mask interferometer" Opt. Lett. **33**, 1449–1451 (2008).

[5] K. Zagorulko, P. Kryukov, Y. Larionov, A. Rybaltovsky, E. Dianov, S. Chekalin, Y. Matveets, and V. Kompanets, "Fabrication of fiber Bragg gratings with 267 nm femtosecond radiation" Opt. Express **12**, 5996–6001 (2004).

[6] N. Groothoff, J. Canning, E. Buckley, K. Lyttikainen, and J. Zagari, "Bragg gratings in air-silica structured fibers" Opt. Lett. **28**, 233–235 (2003).

[7] M. Becker, J. Bergmann, S. Brückner, M. Franke, E. Lindner, M. W. Rothhardt, and H. Bartelt, "Fiber Bragg grating inscription combining DUV sub-picosecond laser pulses and two-beam interferometry" Opt. Express **16**, 19169–19178 (2008).

[8] M. Dubov, I. Bennion, S. A. Slattery, and D. N. Nikogosyan, "Strong long-period fiber gratings recorded at 352 nm" Opt. Lett. **30**, 2533–2535 (2005).

[9] G. Violakis, and S. Pissadakis, *Improved efficiency Bragg grating inscription in a commercial solid core microstructured optical fiber'* (9th International Conference on Transparent Optical Networks, Rome, **2**, pp. 217–220, 1–5 July 2007).

[10] V. Beugin, L. Bigot, P. Niay, M. Lancry, Y. Quiquempois, M. Douay, G. Mélin, A. Fleureau, S. Lempereur, and L. Gasca, "Efficient Bragg gratings in phosphosilicate and germanosilicate photonic crystal fiber" Appl. Opt. **45**, 8186–8193 (2006).

[11] J. Canning, "Gratings and grating devices in structured fibers using 193 nm from an ArF laser" in *Bragg Gratings, Photosensitivity, and Poling in Glass Waveguides: Applications and Fundamentals, OSA Technical Digest Series, Vol. 17* (Optical Society of America, Washington, 2007).

[12] J. Canning, N. Groothoff, K. Cook, C. Martelli, A. Pohl, J. Holdsworth, S. Bandyopadhyay, and M. Stevenson, "Gratings in Structured Optical Fibres" Laser Chem. **2008**, 239417 (2008).

[13] G. D. Marshall, D. J. Kan, A. A. Asatryan, L. C. Botten, and M. J. Withford, "Transverse coupling to the core of a photonic crystal fiber: the photo-inscription of gratings" Opt. Express **15**, 7876–7887 (2007).

[14] T. Geernaert, T. Nasilowski, K. Chah, M. Szpulak, J. Olszewski, G. Statkiewicz, J. Wojcik, K. Poturaj, W. Urbanczyk, M. Becker, M. Rothhardt, H. Bartelt, F. Berghmans, and H. Thienpont, "Fiber bragg gratings in germanium-doped highly birefringent microstructured optical fibers" IEEE Photonic. Tech. L. **20**, 554–556 (2008).

[15] A. J. Taylor, R. B. Gibson, and J. P. Roberts, "Two-photon absorption at 248 nm in ultraviolet window materials" Opt. Lett. **13**, 814–816 (1988).

[16] L. Skuja, "Optically active oxygen-deficiency-related centers in amorphous silicon dioxide" J. Non-Cryst. Solids **239**, 16–48 (1998).

[17] C. M. Smith, N. F. Borrelli, J. J. Price, and D. C. Allan, "Excimer laser-induced expansion in hydrogen-loaded silica" Appl. Phys. Lett. **78**, 2452–2454 (2001).

[18] http://www.sei.co.jp/fbr-opt-eng/submarine/zfiber/zfiber.html

[19] M. Alam, J. Abramczyk, U. Manyam, J. Farroni, and D. Guertin, "Performance of optical fibers in space radiation environment" (6th International Conference on Space Optics, Proceedings of ESA/CNES ICSO 2006, Noordwijk, p. 107.1, 27–30 June 2006).

[20] A. Othonos, and K. Kalli, *Fiber Bragg Gratings: Fundamentals and Applications in Telecommunications and Sensing* (Artech House, Boston, 1999).

[21] http://www.crystal-fiber.com/

[22] C. L. Liou, L. A. Wang, M. C. Shih, and T. J. Chuang, "Characteristics of hydrogenated fiber Bragg gratings" Appl. Phys. A **64**, 191–197 (1997).

[23] S. Pissadakis, M. Livitziis, G. Violakis, and M. Konstantaki, "Inscription of Bragg reflectors in all-silica microstructured optical fibers using 248nm, picosecond, and femtosecond laser radiation" Proc. SPIE **6990**, 69900H (2008).

[24] http://www.optiwave.com

[25] P. Karlitschek, G. Hillrichs, and K.-F. Klein, "Influence of hydrogen on the colour center formation in optical fibers induced by pulsed UV-laser radiation. Part 2: All-silica fibers with low-OH undoped core" Opt. Commun. **155**, 386–397 (1998).

[26] S. Kannan, M. E. Fineman, J. Li, and G. H. Sigel Jr., "Nonuniform distribution of oxygen hole centers in silica optical fibers" Appl. Phys. Lett. **63**, 3440–3442 (1993).

[27] H. Hosono, M. Mizuguchi, L. Skuja, and T. Ogawa, "Fluorine-doped SiO_2 glasses for F_2 excimer laser optics: fluorine content and color-center formation" Opt. Lett. **24**, 1549–1551 (1999).

[28] H. G. Limberger, C. Ban, R. P. Salathé, S. A. Slattery, and D. N. Nikogosyan, "Absence of UV-induced stress in Bragg gratings recorded by high-intensity 264 nm laser pulses in a hydrogenated standard telecom fiber" Opt. Express **15**, 5610–5615 (2007).

[29] A. I. Kalachev, D. N. Nikogosyan, and G. Brambilla, "Long-period fiber grating fabrication by high-intensity femtosecond pulses at 211 nm" J. Lightwave Technol. **23**, 2568–2578 (2005).